Synopsis of the Thesis Entitled

SYNTHESIS OF NOVEL HETEROCYCLES EMPLOYING GREEN PROTOCOLS

Submitted By

A. SHYLAJA, M.Sc.

[Regn. No. F9717]

For the award of DOCTOR OF PHILOSOPHY in Chemistry

Supervisor

Dr. R. RANJITH KUMAR

DEPARTMENT OF ORGANIC CHEMISTRY
SCHOOL OF CHEMISTRY
MADURAI KAMARAJ UNIVERSITY
[*University with potential for excellence*]
['A' grade Accreditation by NAAC – 3rd cycle]
MADURAI - 625 021

November 2019

Chapter 1. Introduction

The first chapter presents a general introduction about the biological significances of heterocyclic scaffolds. The synthesis of various heterocycles employing green protocols such as microwave assisted multicomponent reactions and 1,3-dipolar cycloaddition reactions have been elaborately discussed supported by literature survey.

Chapter 2. Four-Component Domino Synthesis of Pyrazolo[3,4-*h*]quinoline-3-carbonitriles: "Turn-Off" Fluorescent Chemosensor for Fe^{3+} Ions

A series of novel pyrazolo[3,4-*h*]quinoline-3-carbonitriles **5** was synthesized from 1-aryl-1,5,6,7-tetrahydro-4*H*-indazol-4-ones **1**, aromatic aldehydes **2,** malononitrile **3** and ammonium acetate **4** via one pot four component domino protocol under microwave irradiation (**Scheme 1**). The synthesized compounds were characterized with the help of 1 and 2D NMR, IR, HRMS and single crystal X-ray studies**.** The mechanism involves a five-step multiple bond forming transformation *viz*. Knoevenagel condensation–Michael addition–nucleophilic addition to carbonyl–*N*-cyclization–oxidative aromatization sequence leading to the formation of two new C–C and C–N bonds.

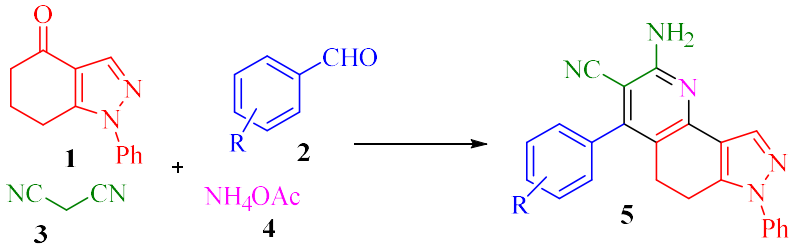

Entry	Comp	Yield	m.p. (^{0}C)
1	**5a**	96	250–253
2	**5b**	94	260–263
3	**5c**	96	275–278
4	**5d**	90	179–181
5	**5e**	88	190–193
6	**5f**	90	266–269
7	**5g**	95	201–203
8	**5h**	90	200–203
9	**5i**	92	195–198
10	**5j**	46	214–217
11	**5k**	50	203–206

Scheme 1. Synthesis of pyrazolo[3,4-*h*]quinoline-3-carbonitriles **5**

Further the analysis of the ^{1}H NMR of all the 5*H*-pyrazolo[3,4-*h*]quinoline-3-carbonitriles revealed that in the cases of **5c–f**, wherein the phenyl ring at C-4 has bulky substitution, the 6-CH_2 protons appeared as distinct multiplets. However, in compounds with *p*-substituted phenyl ring, *viz*. **5a** and **5b**, these protons appeared as a triplet. Presumably, the steric hindrance exerted between the nitrile group at C-3 and the *ortho*-substituted phenyl ring at C-4 restricts the free rotation of the phenyl C–C single bond thereby inducing axial chirality in these molecules (**Figure 2**).

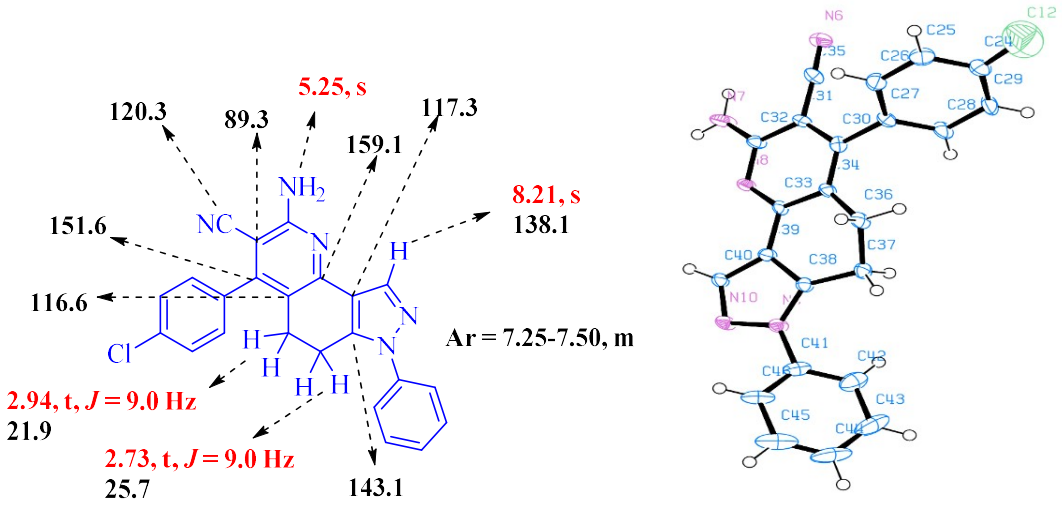

Figure 1. ^{1}H and ^{13}C NMR chemical shift values and ORTEP diagram of **5a**

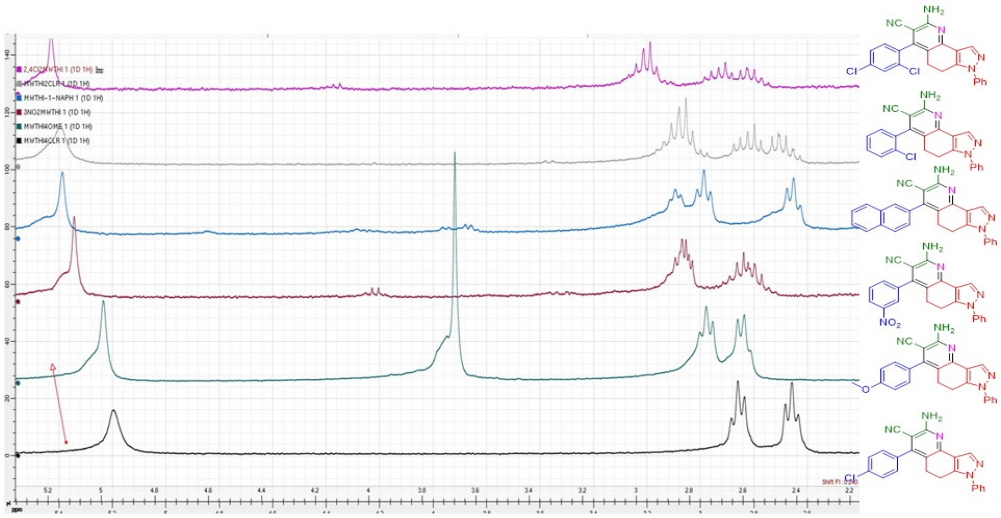

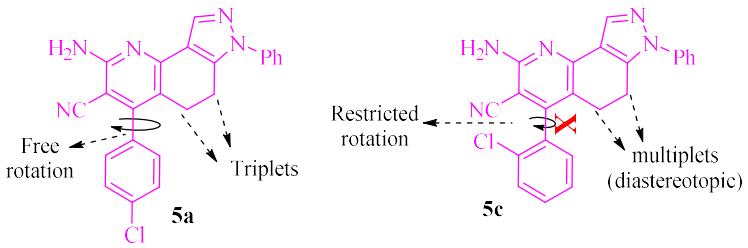

Figure 2. Axial chirality in **5** due to restricted C–C bond rotation

Among the pyrazolo[3,4-*h*]quinoline-3-carbonitriles, compounds **5a–c**, **5e** and **5g** exhibited blue fluorescence under UV lamp. The relative quantum yield of **5** was measured using anthracene in ethanol as standard (**Table 1**). Based on the quantum yield values compound **5b** was chosen as the probe, which was able to selectively detect Fe^{3+} over other metal ions with a detection limit of 8.6×10^{-7} M in DMSO (**Figure 3**). The Stern-Volmer constant (K_{sv}) was found to be 1.5×10^{4} M^{-1}. Fluorescence quenching mechanism involving the inhibition of internal charge transfer by the complexation of probe **5b** and Fe^{3+} ions was proposed based on the DFT studies (**Figure 4**).

Table 1. Relative quantum yield measurement of compounds **5a-g**

Entry	Compound	ΦS
1	**5a**	0.50
2	**5b**	0.60
3	**5c**	0.49
4	**5d**	–
5	**5e**	0.54
6	**5f**	–
7	**5g**	0.37

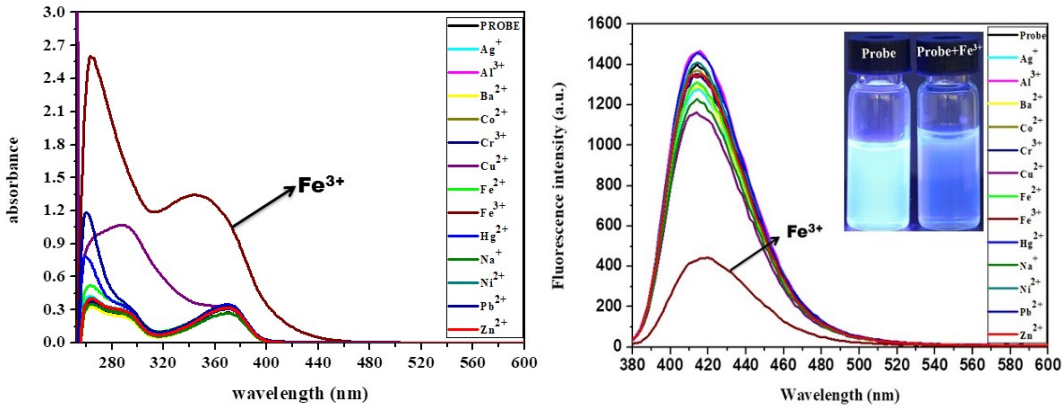

Figure 3. UV and emission spectra of **5b** in the presence of various metal ions

With a view to study the practical applicability of probe **5b**, real sample analyses was performed to determine the concentration of Fe^{3+} in three different water samples. The average recovery of the spiked samples was found to be 109, 94 and 117 respectively for drinking, tap and river water samples. The results show that the probe **5b** successfully quantifies the amount of Fe^{3+} in the water samples (**Table 2**).

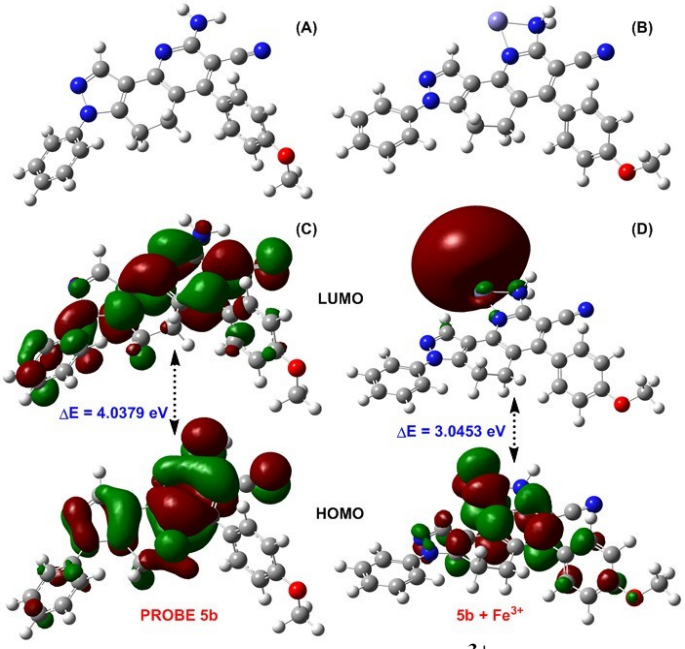

Figure 4. Optimized structure of (A) **5b** and (B) **5b+Fe^{3+}**. Frontier molecular orbital of (C) probe **5b** and (D) **5b+Fe^{3+}**

Table 2. Determination of Fe^{3+} in water samples

Water sample	Fe^{3+} added (µl)	Fe^{3+} found (µl)	Recovery (%)	R.S.D (n=3) (%)
Drinking water (RO treated water taken from the authors Department	0	0	–	–
	30	36	120	1.5
	40	42	105	1.8
	50	51	102	1.0
Tap water (Taken from Velacheri, Chennai)	0	0	–	–
	30	27	90	2.5
	40	41	102	2.4
	50	45	90	1.4
River water (Taken from Thamirabarani river, Tirunelveli)	0	0	–	–
	30	31	103	2.5
	40	50	125	2.8
	50	62	124	2.3

Chapter 3. A One Pot Four Component Synthesis of Blue Emissive Furan Tethered Hybrid Heterocycles for the Dual Detection of Fe^{3+} and Picric Acid

The one-pot four component domino protocol under solvent-free microwave conditions established in Chapter 1 was extended to synthesize 2-amino-4-aryl-6-(2,5-dimethylfuran-3-yl)-pyridine-3-carbonitriles starting from 2,5-dimethyl-3-acetyl furan, aromatic aldehydes, malononitrile and ammonium acetate (**Scheme 2**). These hybrid heterocycles **AFDC**, **AFTB**, **AF3N**, **AF4N** are formed through a similar mechanistic pathway as reported in Chapter 2. The structure of all the derivatives was elucidated unambiguously with the help of 1 and 2 D NMR. The structure was further confirmed by single crystal X-ray studies (**Figure 5**).

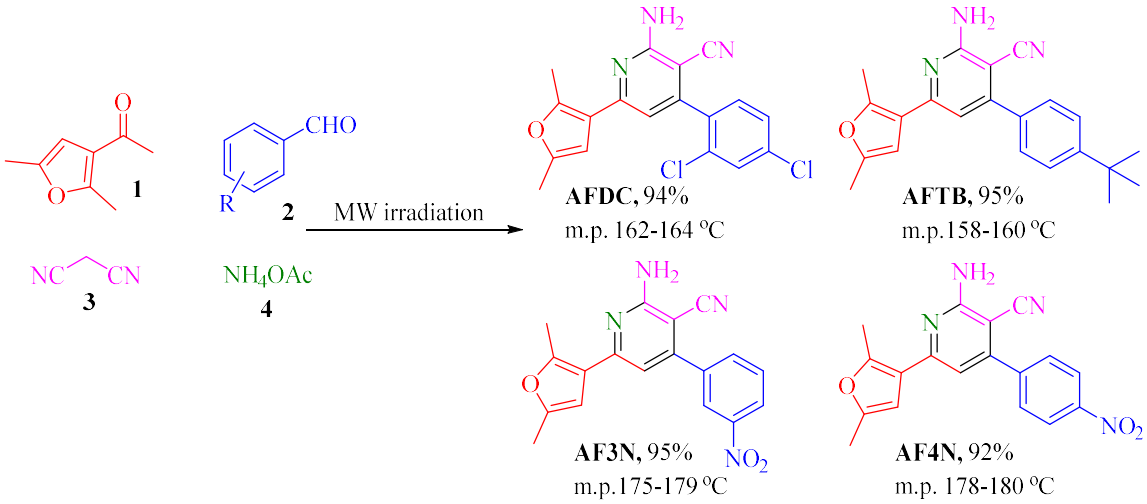

Scheme 2. Synthesis of dimethylfuran-2-aminopyridine-3-carbonitriles

Among the four derivatives the compounds **AFDC** and **AFTB** exhibited fluorescence under UV lamp (**Figure 2**). Based on the relative quantum yield values obtained **AFTB** (Φ = 0.34) was chosen to explore the photophysical applications (**Table 3**). The metal interference studies in both UV and emission revealed that the compound **AFTB** was able to selectively sense Fe^{3+} ions with the detection limit of 4.6 nM by "turn off" mechanism (**Figure 7**). The Stern-Volmer plot revealed the quenching constant Ksv as 1.31×10^4 M^{-1}. With the insight from our previous Chapter, a similar fluorescence quenching mechanism involving the inhibition of

internal charge transfer (ICT) by the complexation of probe **AFTB** and Fe^{3+} ions is proposed based on the DFT studies (**Figure 8**).

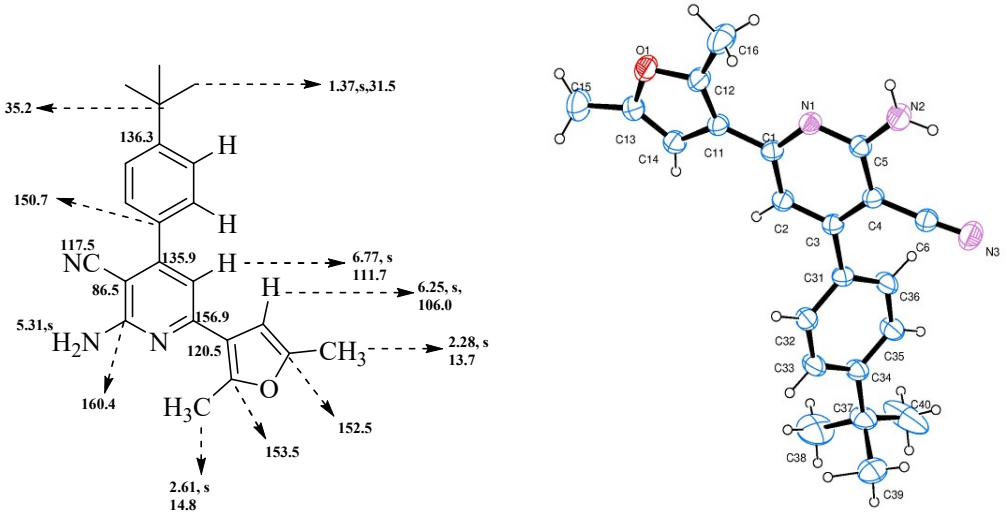

Figure 5. ^{1}H and ^{13}C NMR chemical shift values and ORTEP diagram of **AFTB**

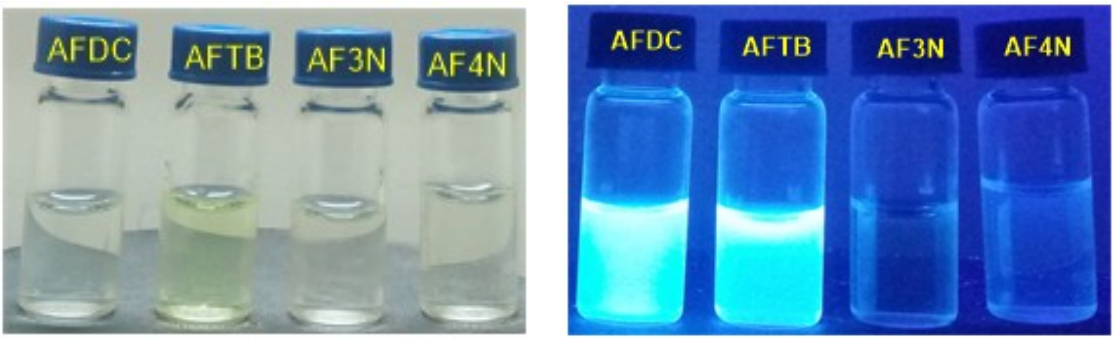

Figure 6. Dimethylfuran-2-aminopyridine-3-carbonitriles under daylight and UV lamp

Table 3. Relative quantum yield of all the compounds

Entry	Compound	Φ_S
1	**AFDC**	0.24
2	**AFTB**	0.34
3	**AF3N**	0.02
4	**AF4N**	0.08

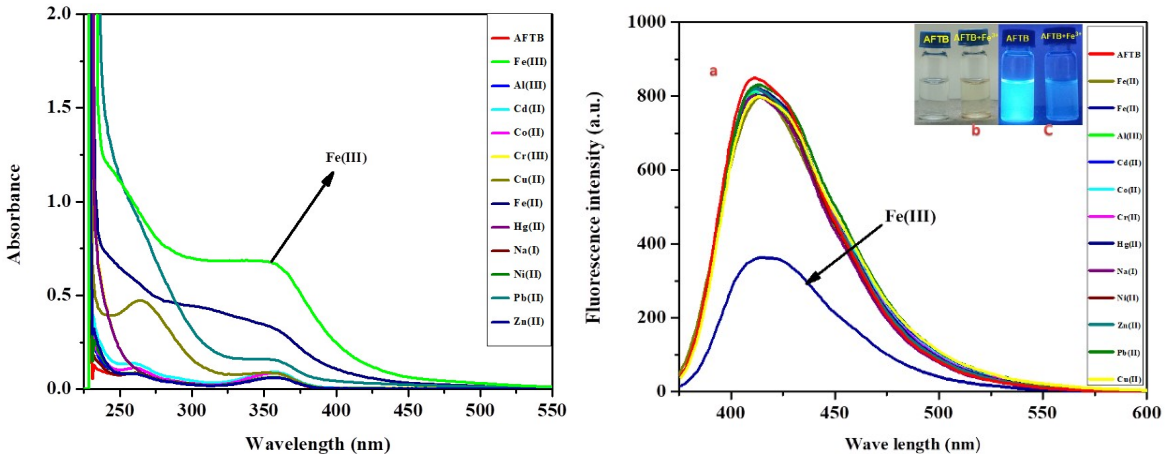

Figure 7. UV and emission spectra (λ_{ex}=354 nm) of the probe **AFTB** in the presence of metal ions (b) **AFTB** and **AFTB**–Fe^{3+} in day light (c) **AFTB** and **AFTB**–Fe^{3+} in UV light

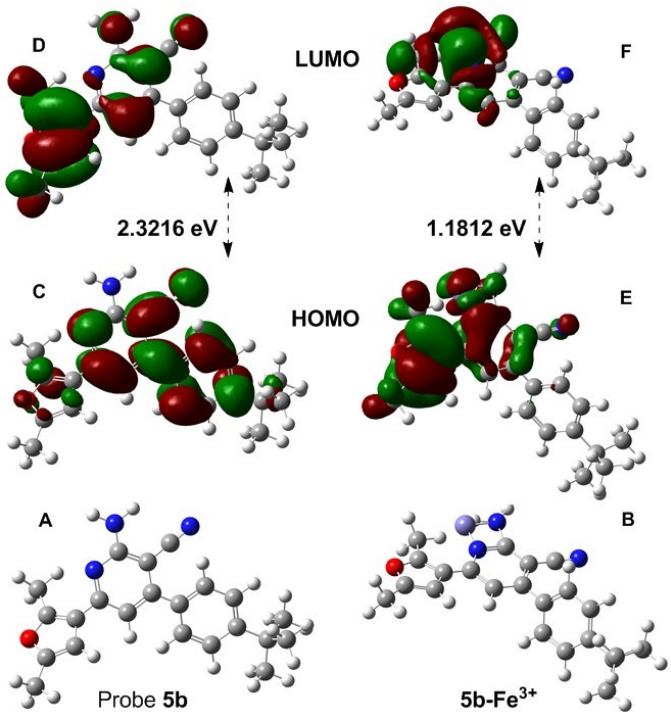

Figure 8. Optimized structure of (A) **AFTB** and (B) **AFTB-**Fe^{3+}; Frontier molecular orbital of (C) probe **AFTB** and (D) **AFTB-**Fe^{3+}

Subsequently the sensing ability of **AFTB** towards organic nitro compounds was also investigated. Among the various nitro compounds the probe **AFTB** selectively detected picric

acid (PA) with a detection limit of 7.9 nM (**Figure 9**). Further the competitive studies revealed the non-interference of other nitro compounds in the presence of PA.

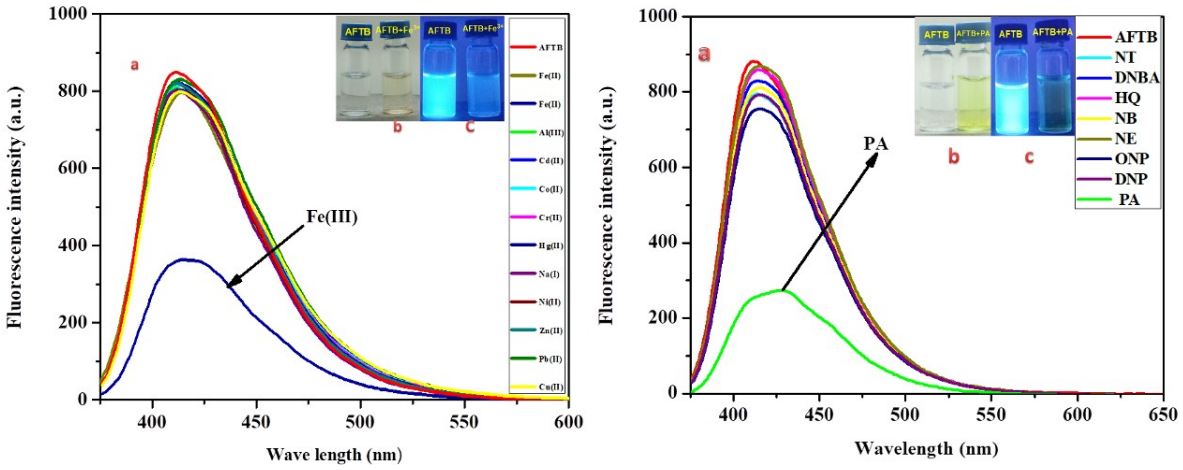

Figure 9. Emission spectra (λ_{ex}=354 nm) of the probe **AFTB** in the presence of metal ions and nitro compounds

In order to find the binding mechanism of PA with the probe **AFTB** NMR titration experiments were carried out. In the ^{1}H NMR spectrum of **AFTB** the free NH_2 protons appeared as a singlet at 5.33 ppm. This signal gradually shifted downfield upon incremental addition of PA starting from 0.3 equiv. into the probe solution and appeared at 6.48 ppm at stoichiometric concentrations (**Figure 10**). Simultaneously, the appearance of a singlet at 9.00 ppm signal due to the aromatic ring protons of PA was also noted. Hence the fluorescence quenching of the probe was attributed to the hydrogen bonding interaction between the NH_2 of the probe **AFTB** and the phenolic OH of PA.

Real sample analyses were also carried out with different Fe^{3+} and PA spiked water samples separately. The average recovery of Fe^{3+} and PA was approximately found to be 95 and 88 % respectively (**Table 4** and **5**).

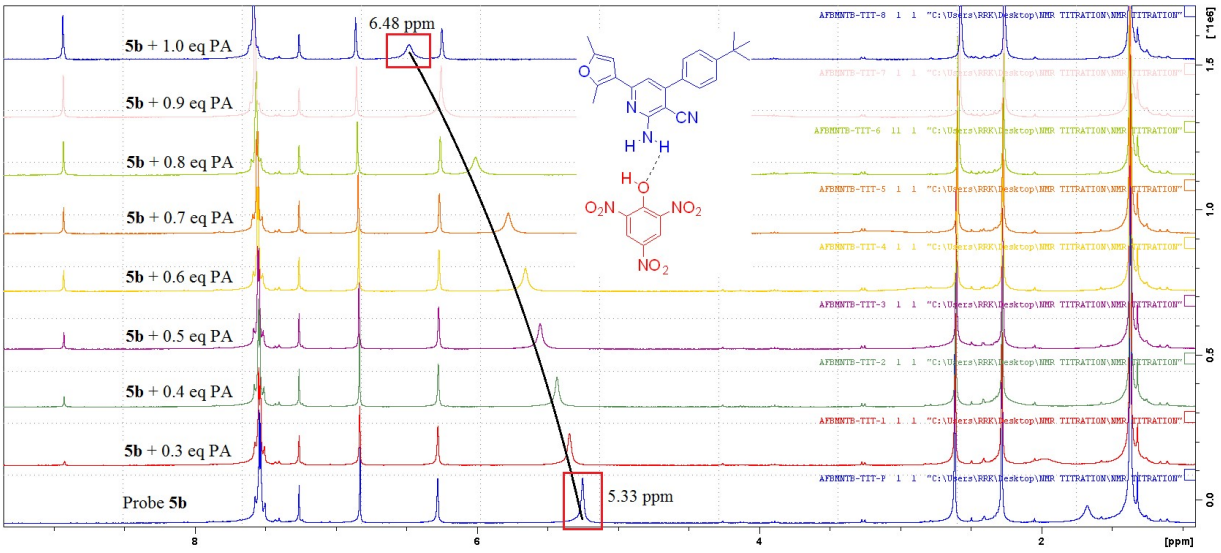

Figure 10. ^{1}H NMR titration experiments of probe **AFTB** with PA

Table 4. Determination of Fe^{3+} in water samples

Water samples	Fe(III) spiked (µl)	Fe(III) found (µl)	Recovery (%)
Thamirabarani river water sample	0	0	-
	30	28	97
	40	37	93
	50	46	94
	60	56	95
Cauvery river water sample	0	0	-
	30	24	90
	40	36	94
	50	44	91
	60	54	92

Table 5. Determination of PA in water samples

Water samples	PA spiked (µl)	PA found (µl)	Recovery (%)
Sea water sample from Chennai	0	0	-
	60	48	89
	70	63	92
	80	65	85
Sea water sample from Thoothukudi	0	0	-
	60	47	81
	70	52	77
	80	57	75

Chapter 4. Green Synthesis and Picric Acid Sensing Studies of Novel Pyrido[2,3-*f*]quinazoline-3-carbonitriles

The microwave-assisted one-pot three-component reaction of 2-phenyl-7,8-dihydroquinazolin-5(6*H*)-one **3**, malononitrile arylidene **6** and ammonium acetate under solvent-free condition occurred through a five-step multiple bond-forming transformation to afford 2-amino-8-phenyl-4-aryl-5,6-dihydropyrido[2,3-*f*]quinazoline-3-carbonitriles in excellent yields (**Scheme 3**). The structure of the synthesized derivatives **7** was elucidated with the help of 1 and 2D NMR spectroscopy (**Figure 11**).

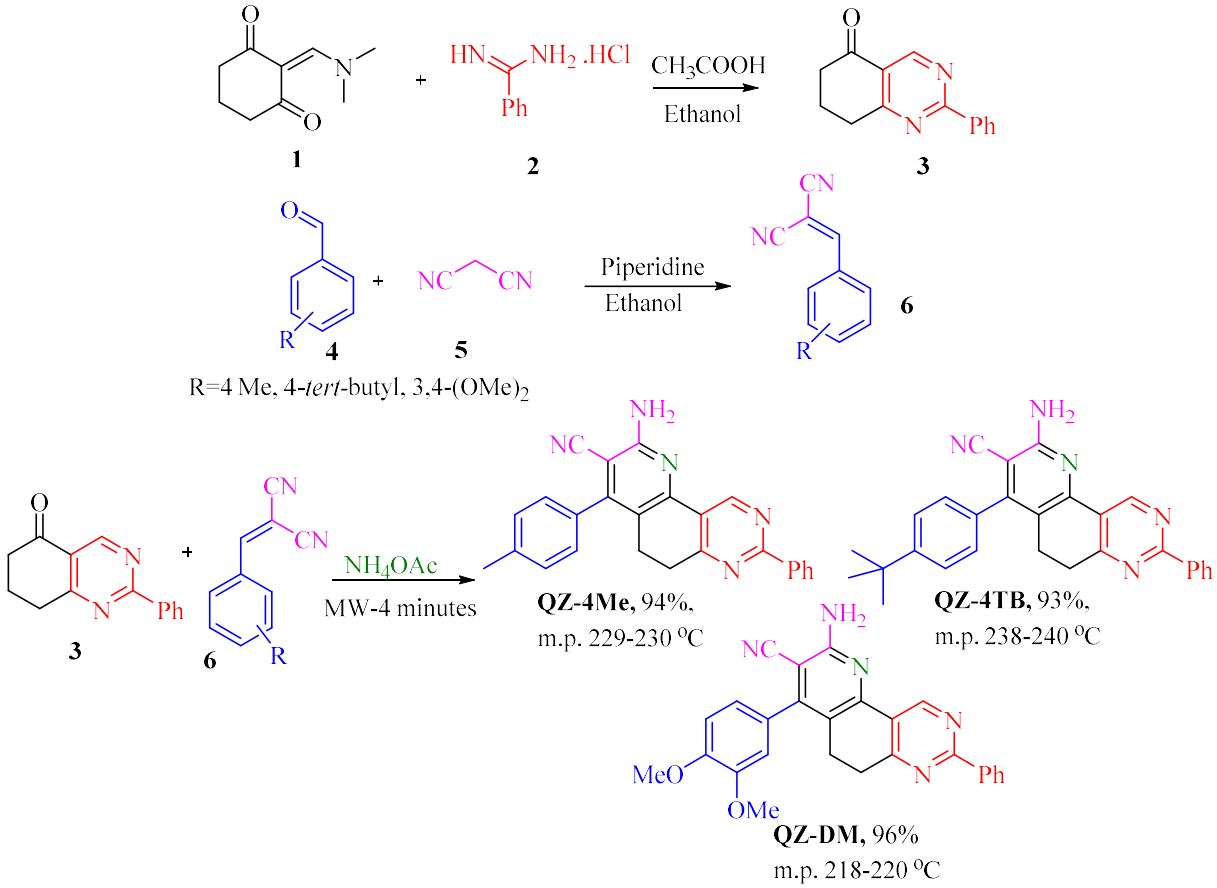

Scheme 3. Synthesis of 2-amino-8-phenyl-4-aryl-5,6-dihydropyrido[2,3-*f*]quinazoline-3-carbonitrile **7**

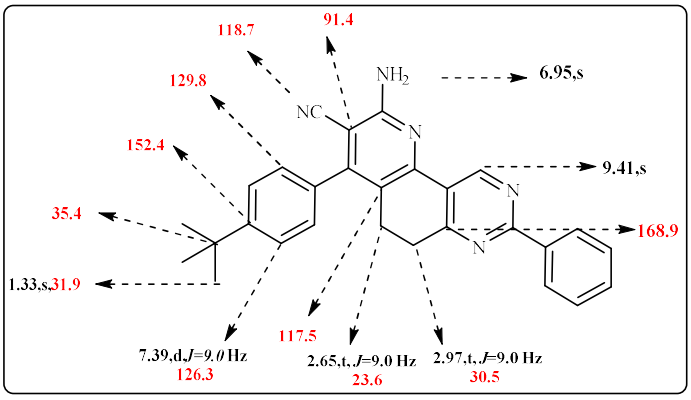

Figure 11. ^{1}H and ^{13}C NMR Chemical shift values of **QZ-4TB**

All the synthesized derivatives **QZ-4Me**, **QZ-4TB**, **QZ-DM** were blue emissive under UV lamp (**Figure 12**) and the relative quantum yield values were calculated (**Table 6**). The metal sensing ability of all the three compounds **QZ-4Me**, **QZ-4TB**, **QZ-DM** was investigated by observing the changes in the UV lamp and emission spectra in the presence of various metal ions in DMSO. The emission spectrum of **QZ-4Me, QZ-4TB, QZ-DM** (20 µM in DMSO) was recorded in the presence of chloride salts of Al^{3+}, Cd^{2+}, Co^{2+}, Cr^{3+}, Cu^{2+}, Fe^{2+}, Fe^{3+}, Hg^{2+}, Ni^{2+}, Pb^{2+} and Zn^{2+} (20×10^{-5} M each in water). However no significant changes in the fluorescence intensity were observed upon addition of all the metal ions including Fe^{3+} (**Figure 13**).

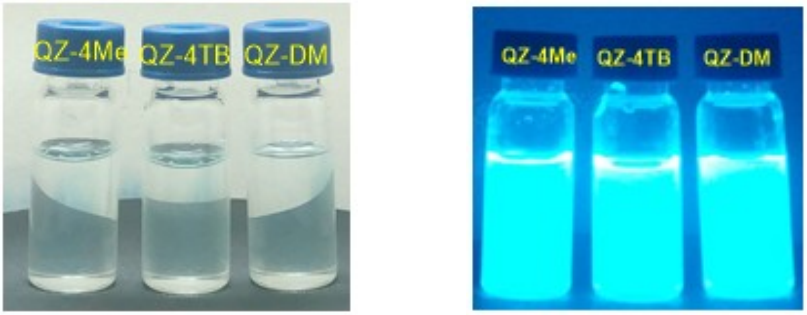

Figure 12. Images of the dihydropyrido[2,3-*f*]quinazoline derivatives in day and UV light

Table 6. Relative quantum yield of all the compounds **7**

Entry	Compound	Φ_S
1	**QZ-4Me**	0.91
2	**QZ-4TB**	0.83
3	**QZ-DM**	0.70

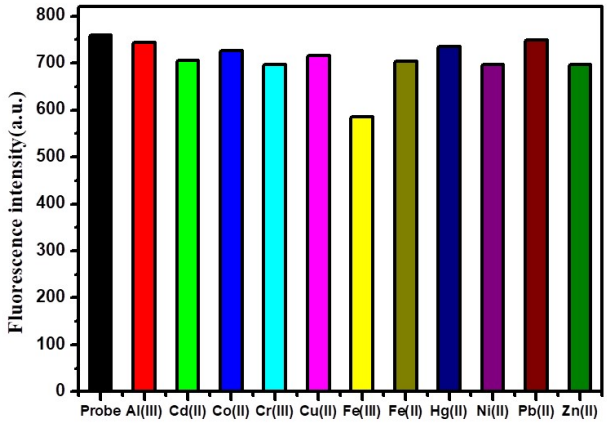

Figure 13. Emission spectra (λ_{ex}=390 nm) of the probe **QZ-4TB (**20 μM) in the presence of metal ions (20× 10^{-5} M)

Further all the probes were tested for sensing PA in both UV as well as emission spectrophotometer in DMSO. The UV absorption spectra of the probe QZ-4Me in the presence of picric acid revealed a significant blue shift and increase in the value of OD. Similarly significant quenching of the fluorescence intensity was observed after the addition of picric acid amidst the other nitro compounds. The UV and emission spectra for the compound **QZ-4TB** are shown in **Figure 14** as the representative case.

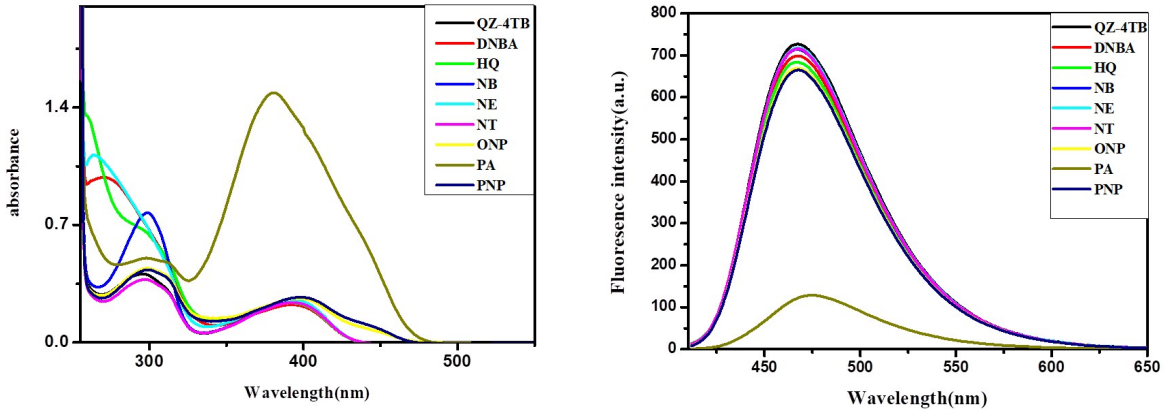

Figure 14. UV and emission spectra of **QZ-4TB** (20 μM) in the presence of various nitro compounds

The quenching constant K_{SV} of **QZ-4TB** calculated from the Stern-Volmer plot was found to be 1.06 ×10^{-5} M. Similarly the lowest limit of detection of PA by the probes **QZ-4TB**

was found to be 1.9 nM. Further the stoichiometric binding ratio of PA with the probes **QZ-4TB** was 1:1 as obtained from the Job's plot. The non-interference of other nitro compounds with the probe against PA was revealed from the competitive studies. The LOD of other two probes **QZ-4Me** and **QZ-DM** was found to be 4.1 and 5.9 nM, respectively.

The real sample analyses with five different PA spiked water samples were analysed with all the three probes **QZ-4Me, QZ-4TB, QZ-DM.** The overall recovery was calculated as 86 to 116%, respectively for all the water samples **(Table 7)**. These inferences disclosed that the probes **QZ-4Me, QZ-4TB, QZ-DM** effectively quantify the amount of PA in the water samples.

Table 7. Determination of PA in water samples by the probes **QZ-4Me, QZ-4TB** and **QZ-DM**

		QZ-4Me			**QZ-4TB**		**QZ-DM**	
S. No	Samples	PA added (μl)	PA found (μl)	Recovery (%)	PA found (μl)	Recovery (%)	PA found (μl)	Recovery (%)
	Sea water samples							
1	Thoothukudi							
		5	6	95	6	90	3	103
		10	10	100	9	106	9	95
		15	14	107	15	103	12	99
2	Thiruchenthur							
		5	4	96	3	104	3	100
		10	8	107	6	111	9	86
		15	14	105	12	97	12	88
3	Mannapadu							
		5	4	101	3	95	6	98
		10	8	99	9	102	9	116
		15	14	101	15	104	15	102
4	Marina							
		5	6	102	3	89	3	99
		10	10	98	9	101	6	110
		15	16	95	15	103	12	96
	River water sample							
5	Thamirabharani							
		5	4	101	3	104	3	96
		10	8	102	6	108	6	112
		15	12	99	9	102	12	100
	Tap water sample							
6	Madurai							
		5	4	92	3	87	3	103
		10	8	102	9	100	9	98
		15	14	85	15	100	15	86

Chapter 5. Phenothiazine Tethered Spiro Pyrrolidine/Pyrrolothiazole–Oxindole/Acenaphthene/ indeno[1,2-*b*]quinoxaline Hybrids: Combinatorial Synthesis and Photophysical Studies

The dipolarophiles *viz*. (*E*)-1-(10*H*-phenothiazin-2-yl)-3-arylprop-2-en-1-ones **3** were synthesized from the base promoted Knoevenagel condensation of 2-acetyl phenothiazine **1** and aromatic aldehydes **2** (**Scheme 4**).

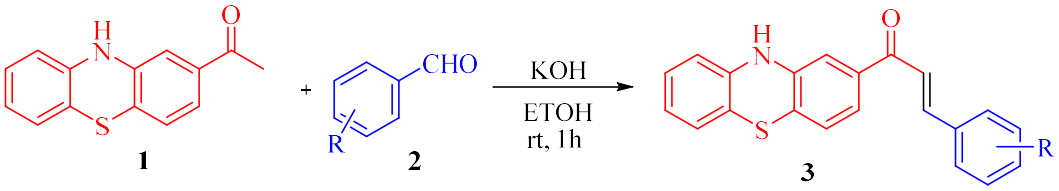

Scheme 4. Synthesis of (*E*)-1-(10*H*-phenothiazin-3-yl)-3-arylprop-2-en-1-ones **3**

Subsequently the synthesis of phenothiazine tethered spiro pyrrolidine/pyrrolothiazole–oxindole/acenaphthene/indeno[1,2-*b*]quinoxalines hybrid heterocycles **6–14** was achieved via the 1,3-dipolar cycloaddition of azomethine ylides generated *in situ* from isatin/acenaphylene-1,2-dione/indeno[1,2-*b*]quinoxalines **4** and sarcosine/phenyl glycine/thiazolidine-4-carboxylic acids **5** (**Scheme 5**). The structure of the phenothiazine tethered spiro derivatives was elucidated with the help of 1 and 2D NMR spectroscopy and single crystal X-ray analysis (**Figure 15**).

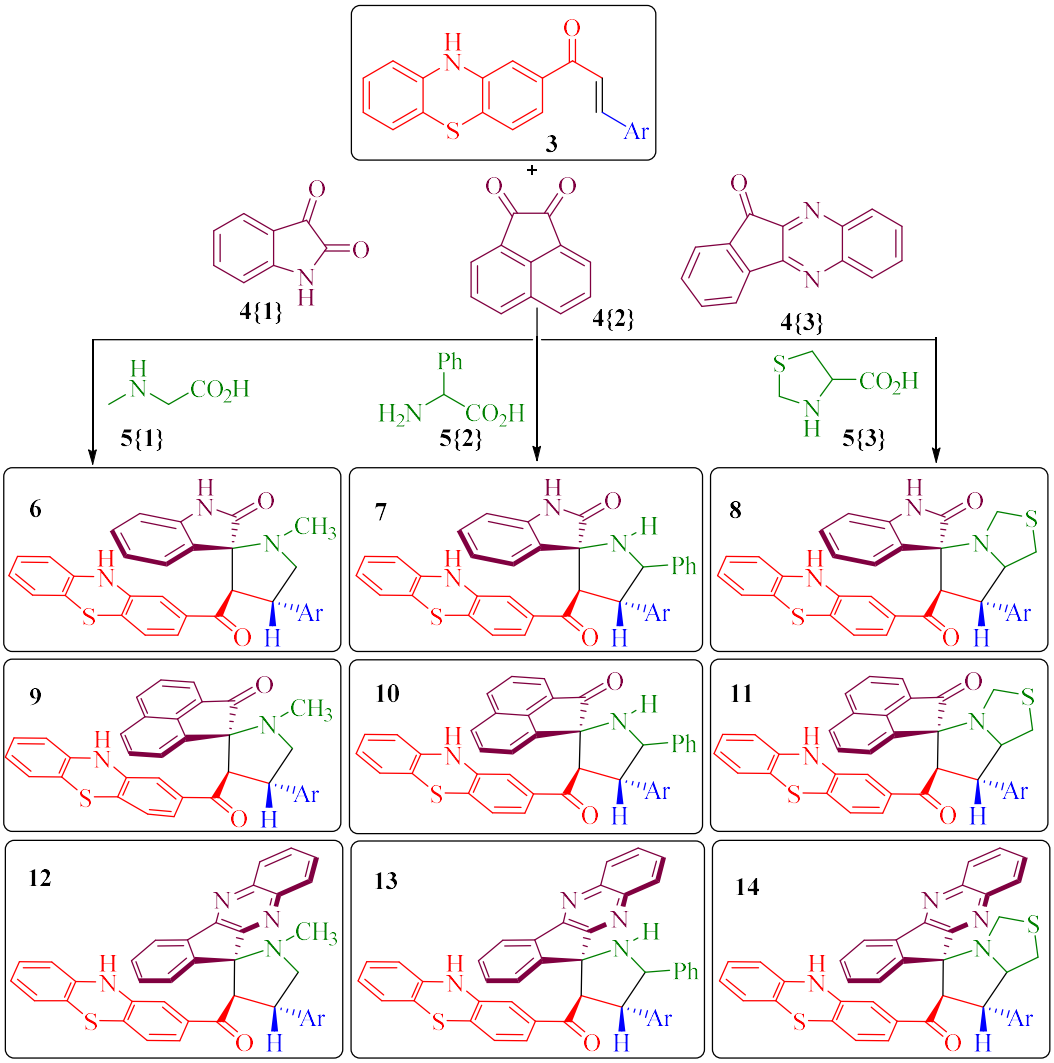

Entry	Comp	Ar	Yield (%) and melting point (^{0}C)								
			6	7	8	9	10	11	12	13	14
1	**a**	4-ClC_6H_4	96	93	92	94	95	96	93	94	95
2	**b**	4-MeC_6H_4	92	91	90	93	94	92	91	91	94
3	**c**	2,4-$Cl_2C_6H_3$	94	90	94	93	92	92	92	90	94
4	**d**	4-FC_6H_4	94	92	90	92	93	90	89	91	90

Scheme 5. Library of phenothiazine tethered spiro hybrid heterocycles

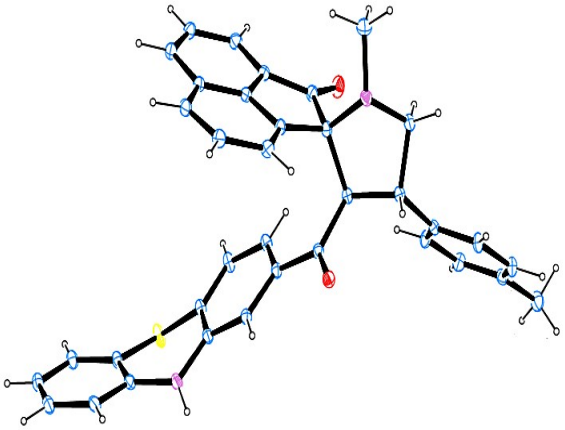

Figure 15. ORTEP diagram of **11b**

Among the phenothiazine tethered spiro pyrrolidine/pyrrolothiazole–oxindole/ acenaphthene/indeno[1,2-*b*]quinoxaline derivatives **6–14**, the twelve isatin derived spiro hybrids **6-8** exhibited fluorescence under UV lamp. Hence all the twelve compounds were subjected to photophysical studies in both UV and emission spectrophotometer. The solvatochromism properties were studied in various solvents ranging from non-polar to polar solvent such as toluene, chloroform, tetrahydrofuran (THF), dimethylsulfoxide (DMSO) and acetonitrile (ACN) (**Figure 16**). A positive solvatochromic shift was observed in the emission spectroscopy from 520 – 600 nm and stokes shift was calculated from both UV and emission spectra. In addition relative quantum yield measurements were also done in all the solvents mentioned above. Based on the relative quantum yield values in DMSO, compound **7c** was chosen as the probe for the metal sensing studies. Among the various metals, Fe^{3+} selectively quenches the fluorescence intensity of the compound **7c** with a detection limit of 6.4×10^{-7} M in DMSO (**Figure 17**).

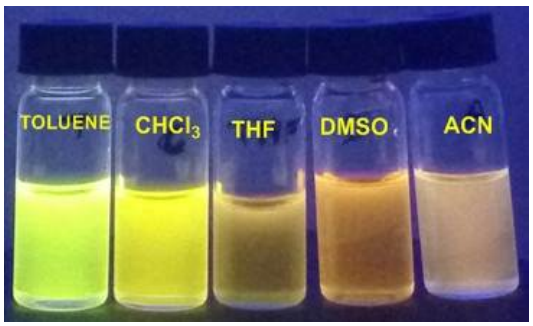

Figure 16. Photographs of the isatin derived compounds in different solvents

Table 9. Relative quantum yield of the compounds **6-8** in various solvents

Comp	Φ_S				
	Toluene	**$CHCl_3$**	**THF**	**DMSO**	**ACN**
6a	0.19	0.59	0.06	0.18	0.54
6b	0.17	0.81	0.004	0.30	0.63
6c	0.01	0.93	0.02	0.18	0.24
6d	0.27	0.76	0.06	0.11	0.45
7a	0.14	0.60	NIL	0.15	0.44
7b	0.15	0.62	0.22	0.29	0.59
7c	0.10	0.89	0.02	0.31	0.55
7d	0.16	0.92	0.38	0.15	0.32
8a	0.23	0.64	0.08	0.11	0.41
8b	0.18	0.75	0.005	0.25	0.56
8c	0.12	0.54	NIL	0.16	0.29
8d	0.20	0.42	0.02	0.08	0.16

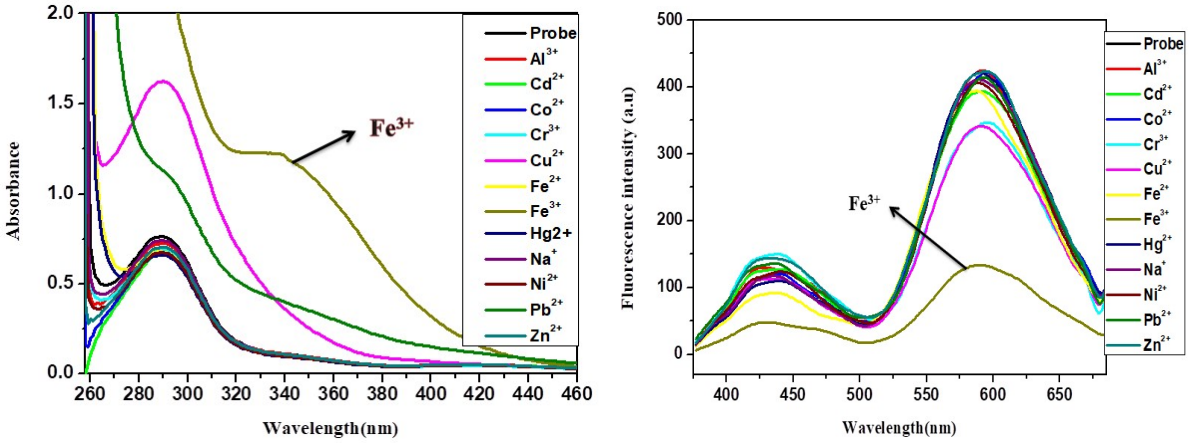

Figure 17. UV and emission spectra of **7c** (30 μM) in the presence of various metal ions (15×10^{-5} M) in DMSO

Chapter 6. Dimethylfuran Tethered Spiro Pyrrolidine/Pyrrolo[1,2-*c*]thiazolo–Oxindole/ Acenaphthalene Hybrid Heterocycles: Synthesis and Antioxidant Studies

A library of novel furan tethered pyrrolidine/pyrrolo[1,2-*c*]thiazolo–oxindole/ acenaphthalene hybrid heterocycles **9** and **11-14** were synthesized via 1,3-dipolar cycloaddition of azomethine ylides generated in situ from the reaction of isatin **4**/acenaphylene-1,2-dione **5** and sarcosine **6**/phenylglycine **7**/thiazolidene-4-carboxylic acid **8** to the dipolarophile *viz*. 2,5-dimethyl furan **3** (**Schemes 6–7** and **Table 10**). All the synthesized compounds were well characterized by 1 and 2D NMR spectroscopy.

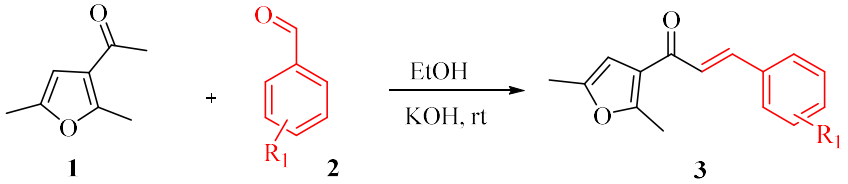

Scheme 6. Synthesis of (*E*)-1-(2,5-dimethylfuran-3-yl)-3-phenylprop-2-en-1-one **3**

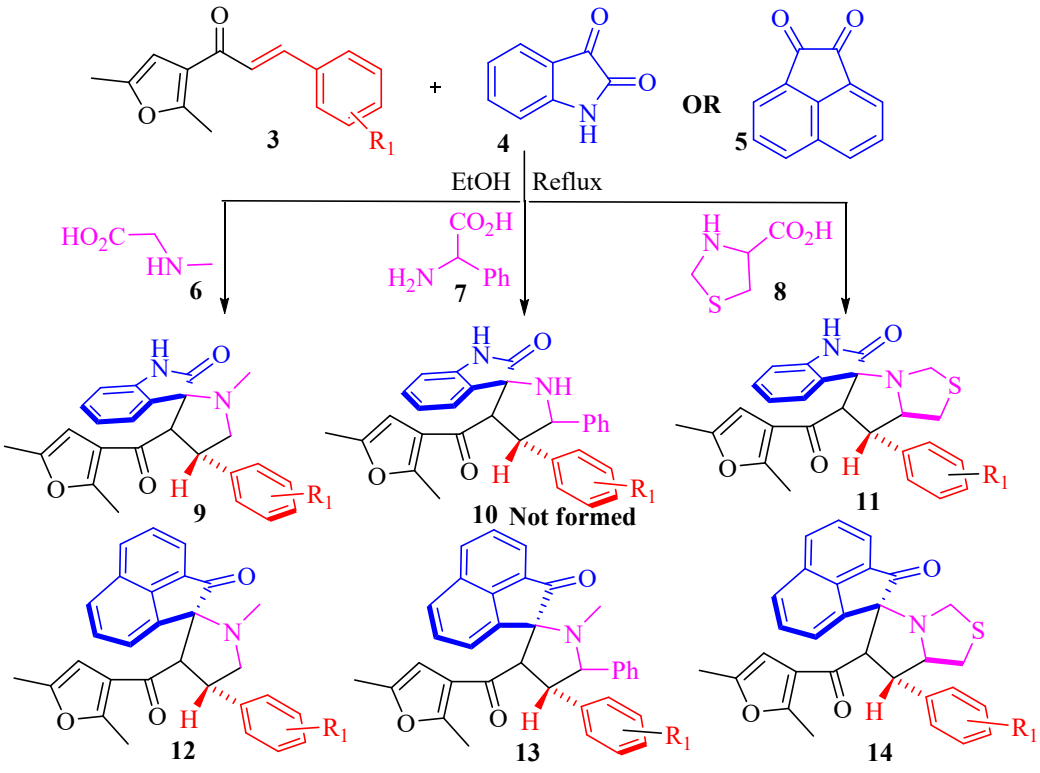

Scheme 7: Library of furan tethered spiro hybrid heterocycles

Table 10: Yield and melting point of the compounds **9** and **11-14**

Entry	Comp	R_1	Yield (%) and melting point (^{0}C)				
			9	**11**	**12**	**13**	**14**
1	**a**	4-Cl	90 143-146	92 113-116	94 141-143	90 149-152	95 104-107
2	**b**	4-Me	94 159-162	94 120-123	93 139-142	91 190-193	94 150-153
3	**c**	2,4-Cl_2	92 178-181	93 150-153	93 118-121	92 125-128	94 110-113
4	**d**	3-NO_2	89 203-206	88 193-196	90 123-126	89 138-141	90 134-137

All the compounds **9** and **11-14** were subjected to DPPH antioxidant assay and their percentage of radical scavenging activity (% RSA) was determined (**Figure 18**). Among the twenty compounds, compounds **14a** (58%)**, 14b** (49%), **11c** (38%)**, 14d** (28%) and **11a** (27%) showed higher radical scavenging activity than the remaining compounds and hence it was concluded that the compounds with pyrrolothiazole core exhibited potent radical scavenging activity.

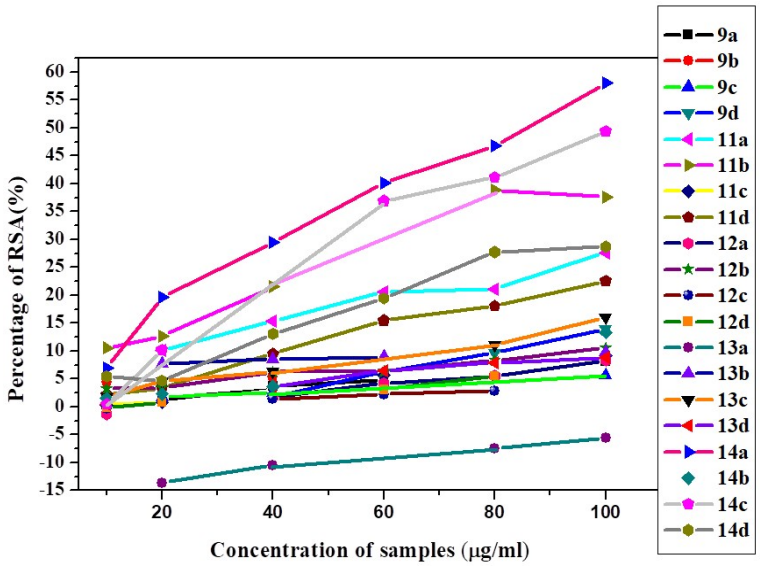

Figure 18: Radical scavenging activities of all the synthesized compounds